
Optimized Sparse Matrix Operations for Reverse Mode Automatic Differentiation

Nicolas Nytko¹ Ali Taghibakhshi² Tareq Uz Zaman³ Scott MacLachlan⁴ Luke N. Olson¹ Matt West²

Abstract

Sparse matrix representations are ubiquitous in computational science and machine learning, leading to significant reductions in compute time, in comparison to dense representation, for problems that have local connectivity. The adoption of sparse representation in leading ML frameworks such as PyTorch is incomplete, however, with support for both automatic differentiation and GPU acceleration missing. In this work, we present an implementation of a CSR-based sparse matrix wrapper for PyTorch with CUDA acceleration for basic matrix operations, as well as automatic differentiability. We also present several applications of the resulting sparse kernels to optimization problems, demonstrating ease of implementation and performance measurements versus their dense counterparts.

1. Introduction

The popularity of automatic differentiation (AD) support in libraries such as PyTorch (Paszke et al., 2019), Tensorflow (Abadi et al., 2016), or Jax (Bradbury et al., 2018) has exploded in recent years, allowing rapid development of models and optimization problems without requiring analytical gradients before training. These libraries allow taking the gradient of complex chains of operations by decomposing them into small, atomic operations then linking them together by copious usage of the chain rule. As an example, differentiation through traditional matrix-matrix multiplication or matrix addition is straightforward and efficient.

While dense matrix linear algebra routines are readily implemented and available in these frameworks, their sparse

counterparts have received less attention. In the case of PyTorch, Tensorflow, and Jax, all three have only preliminary support for sparse matrices stored in the coordinate (COO) format and cannot auto-differentiate through standard sparse matrix operations such as matrix-matrix multiplication.

However, the use of sparse linear algebra is extensive in computational science, for example in the solution to partial differential equations (PDEs) (Briggs et al., 2000; Saad, 2003), circuit analysis (Bonfatti et al., 1973), and graph neighborhood analysis (Saad, 2003; George et al., 1993), among many others, motivating the need for a more complete treatment of sparse operations. Moreover, there is growing demand for sparse kernels in the broader area of scientific machine learning (SciML), where machine learning techniques augment traditional scientific computing methods. The authors in Greenfeld et al. (2019); Luz et al. (2020) learn methods to accelerate linear system solution algorithms but they need to develop various simplifications in the problems themselves due to the lack of sparse linear algebra routines with automatic differentiation. Similarly, the method presented in Taghibakhshi et al. (2022) is constrained to training on small problems because they were forced to treat their sparse matrices as dense to allow for automatic differentiation. We thus seek an implementation of such sparse routines to allow machine learning researchers and computational scientists to develop scalable, learned methods.

The main contributions we make in this paper are structured as follows:

1. construction of reverse mode gradients for several sparse operations and their implementation on both CPU and GPU (CUDA) processors in Section 2, as well as an open-sourced implementation for PyTorch,
2. application to several optimization problems in Section 3, including use of graph neural networks (Wu et al., 2021; Kipf & Welling, 2017) to motivate the use of differentiable sparse kernels, where the problem would be intractable with existing dense implementations, and
3. performance results for the applications of sparse optimization, showing improved performance and scalabil-

¹Department of Computer Science, University of Illinois at Urbana-Champaign ²Department of Mechanical Science and Engineering, University of Illinois at Urbana-Champaign ³Scientific Computing Program, Memorial University of Newfoundland ⁴Department of Mathematics and Statistics, Memorial University of Newfoundland. Correspondence to: Nicolas Nytko <nnytko2@illinois.edu>.

Table 1. Definitions of vector-Jacobian products (VJP) for the different sparse operations. The vector in the VJP (denoted by v or V) is the intermediate gradient with respect to (WRT) the output of the operation when running backpropagation.

METHOD	OPERATION	WRT	VJP
SPMV	Ax	A	$vx^T \odot \text{mask}(A)$
SPMV	Ax	x	$A^T v$
SPSPMM	AB	A	$(VB^T) \odot \text{mask}(A)$
SPSPMM	AB	B	$(A^T V) \odot \text{mask}(B)$
SPDMM	AB	A	$(VB^T) \odot \text{mask}(A)$
SPDMM	AB	B	$A^T V$
SP + SP	$\alpha A + \beta B$	A	$\alpha V \odot \text{mask}(A)$
SP + SP	$\alpha A + \beta B$	B	$\beta V \odot \text{mask}(B)$
SPSOLVE	$x = A^{-1}b$	A	$-A^{-T}vx^T \odot \text{mask}(A)$
SPSOLVE	$x = A^{-1}b$	b	$A^{-T}v$

ity for recent methods such as the domain decomposition method from Taghibakhshi et al. (2022).

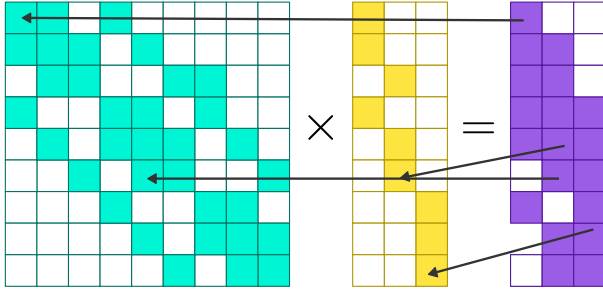


Figure 1. Back-propagation through a sparse matrix-matrix multiplication. Gradient information flows from nonzero entries in the output to nonzero entries in the input.

2. Sparse Kernels

For this work, we implement optimized forward and backward passes (vector-Jacobian product (VJP) implementations) for various sparse operations (see Table 1) with an underlying compressed sparse row (CSR) data structure (see Section 2.1). We propagate *sparse* gradients (Figure 1) whereby functions that take sparse inputs will have gradients whose sparsity mask will match those of the inputs. This trade-off leads to much smaller memory and computational costs (as observed indirectly in Table 4) as, during optimization, only nonzero entries in the inputs will receive gradients. For example, optimizing a problem with a sparse-matrix input and scalar output will only lead to optimization of the nonzero entries of the input.

We next detail the forward and backward implementation

(also known as VJP) of several sparse operations; for a review on backpropagation and automatic differentiation, see Appendix B. For derivations of the matrix reverse-mode updates, we point the reader to Giles (2008) and remark that with minor consideration of the sparsity patterns, the results extend to sparse matrices. For timing results detailing the speedup over dense operations that is obtained, see Appendix C. The reference implementation for all of the following routines is released as an open-sourced library for PyTorch whose code can be downloaded from <https://github.com/nicknytko/numml>.

2.1. Compressed Sparse Row format

The *compressed sparse row* (CSR) format is a row-oriented representation for storage of sparse matrices (Saad, 2003). In this representation, three arrays are needed to determine a single sparse matrix, $A \in \mathbb{R}^{m \times n}$. Denoting $\text{nnz}(A)$ as the number of nonzero entries in A , the three arrays become:

- `data` of size $\text{nnz}(A)$ storing nonzero data entries sorted in row then column order,
- `indices` of size $\text{nnz}(A)$ storing the column number of each respective nonzero entry, and
- `indptr` of size $n + 1$ that stores the *offset* into `data` of the starting point of each row.

By convention, the last entry of `indptr` stores the number of nonzeros in A .

We use the CSR representation in this work because it provides regular, cache-friendly memory access to the matrix rows; this is especially useful in products where the matrix is left-multiplying, for example in the sparse matrix-vector product Ax or sparse-times-dense matrix product AD , where A is sparse and x , D are a dense vector and matrix, respectively.

2.2. Sparse Matrix-Vector (SpMV)

The sparse matrix-vector product computes

$$y \leftarrow Ax \quad (1)$$

for sparse $A \in \mathbb{R}^{m \times n}$, dense $x \in \mathbb{R}^n$, and outputs $y \in \mathbb{R}^m$. The CSR representation allows for direct evaluation of inner products of each row of A and x , and the inner products can be executed in parallel on a GPU.

For the backward pass, we compute $A^T v$ (resp. vx^T) for the gradient with respect to x (resp. A), for intermediate gradient value v . This does not directly align with the sparse structure; hence, we use the reduction-based algorithm as outlined in Tao et al. (2014): inner products of the rows of A and v are computed and atomically reduced into correct entries in the output vector. Computing vx^T is easily parallelized, since it is the outer product between two dense

vectors that is masked to a sparse matrix, requiring computation of only nonzero entries of A .

2.3. Sparse-Sparse Matrix Multiply (SpSpMM)

For the sparse-sparse matrix multiply primitive, we compute

$$C \leftarrow AB, \quad (2)$$

where $A \in \mathbb{R}^{m \times n}$, $B \in \mathbb{R}^{n \times p}$, and $C \in \mathbb{R}^{m \times p}$, with all three matrices stored in CSR format. In the forward pass, we follow the parallel SpGEMM algorithm from Dalton et al. (2015), where we compute intermediate products of each row of A and the entirety of B , then reduce and collect redundant entries to form C .

For the backward pass, we compute $(VB^T) \odot \text{mask}(A)$ and $(A^T V) \odot \text{mask}(B)$. Noting that the product VB^T is the inner product between rows of both V and B , our data accesses aligns directly with the CSR structure. Computing $A^T V$, however, accesses columns of both A and V ; we thus follow a modified version of the SpGEMM algorithm from above that operates on columns of A instead.

2.4. Sparse-Dense Matrix Multiply (SpDMM)

For the SpDMM routine, we compute

$$C \leftarrow AB \quad (3)$$

as in the SpSpMM case except for B and C now being dense. In the forward pass, we parallelize with each fine-grained operation focusing on an entry of C . That is, we compute the respective inner product between a row of A and a column of B which, because of its dense structure, does not incur any significant penalties for column accesses.

On the backward pass, we compute $(VB^T) \odot \text{mask}(A)$ (as before) and $A^T V$. For the latter, we take the sparse transpose of A and re-execute the forward routine to compute the gradient.

2.5. Sparse + Sparse

In a sparse add, we compute the linear combination of two sparse matrices as in

$$C \leftarrow \alpha A + \beta B, \quad (4)$$

which we write in a general form so that both $A + B$ and $A - B$ can be computed with the same method. A key observation is that (with slight abuse of notation),

$$\text{mask}(C) = \text{mask}(A) \cup \text{mask}(B), \quad (5)$$

meaning the computation of C can be viewed as a union over the rows of A and B . Moreover, this form can be implemented in parallel over each row.

To compute the backward pass, we consider the gradient with respect to A , B as $\alpha V \odot \text{mask}(A)$, $\beta V \odot \text{mask}(B)$, respectively. Each can be found as the row-wise reduction from V to the sparsity mask of A or B . Because both $\text{mask}(A)$, $\text{mask}(B) \subseteq \text{mask}(V)$, we need only to compute matching nonzero entries in both matrices, which can again be implemented in parallel over the rows.

2.6. Sparse Triangular Solve

A sparse triangular solve is an operation to compute the value of x in the matrix equation

$$Lx = b, \quad (6)$$

where L has a lower triangular form, i.e. $l_{ij} \neq 0$ if $i \geq j$. Without loss of generality, we can also consider upper-triangular systems U using matrix flip operations to convert $Ux = b$ into an equivalent lower-triangular system. Such a system has a (relatively) simple routine for computing the linear solve: each row depends on the intermediate values of previous rows only and no intermediate preprocessing is needed.

For the forward pass, we elect to use the synchronization-free GPU triangular solve from Su et al. (2020) to exploit the limited parallelism that may exist in computing x .

On the backward pass, we can refer to the general VJP rule for a sparse linear solve; we seek $L^{-T}v$ and $-L^{-T}vx^T \odot \text{mask}(L)$ for gradients with respect to b and L , respectively. We first find $L^{-T}v$ with our existing forward triangular solve routine. We then observe that the gradient with respect to L contains the b gradient term as a masked outer product, so we can re-use the result. The masked outer-product can be executed in parallel over the nonzero entries of L .

3. Applications of Sparse Kernels

To demonstrate the use of the sparse kernels and differentiability above, we present several optimization problems that exercise sparse-matrix computations. As an example sparse matrix, we define $A \in \mathbb{R}^{n \times n}$ as

$$A = \begin{bmatrix} 2 & -1 & & & \\ -1 & \ddots & \ddots & & \\ & \ddots & \ddots & -1 & \\ & & & -1 & 2 \end{bmatrix}, \quad (7)$$

which is a standard test problem in computational science and comes from the finite-difference discretization of the 1D Poisson problem (Saad, 2003; Quarteroni et al., 2006),

$$-\nabla^2 u = f \quad \text{in } \Omega, \quad (8)$$

$$u = 0 \quad \text{on } \partial\Omega, \quad (9)$$

on the domain $\Omega = (0, n + 1) \subseteq \mathbb{R}$, with n being the number of interior gridpoints in the discretization — the domain is selected to cancel any constant scaling of the matrix. This results in a constant number of nonzero entries per row (3) away from the boundary.

The remainder of this section describes several problems that involve heavy use of sparse operations. Corresponding timings for each of these examples are included in Section 4, along with comparison to timings using only dense operations. In each of the problems below, we optimize using the Adam optimizer (Kingma & Ba, 2014) and compute gradients with PyTorch’s automatic differentiation and our sparse kernels.

3.1. Entry-wise Jacobi Relaxation

The Jacobi method is an iterative solver for linear systems whereby the inverse matrix is approximated by inverting the diagonal entries only (Saad, 2003). Consider solving

$$\mathbf{A}\mathbf{x} = \mathbf{b}, \quad (10)$$

where $\mathbf{A} \in \mathbb{R}^{n \times n}$ is a sparse matrix with diagonal \mathbf{D} . The Jacobi method is expressed as

$$\mathbf{x}^{(k+1)} = \mathbf{D}^{-1} \left(\mathbf{b} - (\mathbf{A} - \mathbf{D}) \mathbf{x}^{(k)} \right), \quad (11)$$

though in practice this can often see slow convergence towards a solution.

Convergence can be accelerated by separately weighting the previous value of \mathbf{x} and the approximate inverse at each iteration; here, we consider the case where this weighting is determined independently for each entry of \mathbf{x} . Denoting Ω as the diagonal scaling matrix of the entries of $\mathbf{x}^{(k)}$, we then rewrite the Jacobi iteration as

$$\mathbf{x}^{(k+1)} = \Omega \mathbf{D}^{-1} \mathbf{b} + (\mathbf{I} - \Omega \mathbf{D}^{-1} \mathbf{A}) \mathbf{x}^{(k)}. \quad (12)$$

To simplify the notation, we write $\mathbf{j}(\mathbf{x}_0, \mathbf{b}; \Omega)$ as the function that applies one iteration of the weighted Jacobi scheme to \mathbf{x}_0 in order to solve $\mathbf{A}\mathbf{x} = \mathbf{b}$.

We generate a finite-difference matrix \mathbf{A} from Equation (7) of size $n = 16$, then optimize the entries of Ω by minimizing

$$\ell = \sum_{k=1}^K (\mathbf{j}(\mathbf{x}_k, \mathbf{0}; \Omega))^T \mathbf{A} \mathbf{j}(\mathbf{x}_k, \mathbf{0}; \Omega), \quad (13)$$

where $\{\mathbf{x}_1, \mathbf{x}_2, \dots, \mathbf{x}_K\}$ are a set of test vectors in \mathbb{R}^n with random unit-normally distributed entries. This optimizes the one-step Jacobi error when solving for a $\mathbf{0}$ right-hand side.

Training loss history and final values of the weights are shown in Figures 2 and 3. In Figure 3, we observe that the

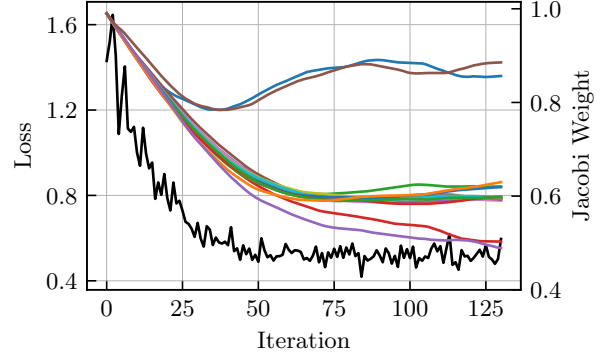


Figure 2. Loss history (in black) obtained from optimizing over the Jacobi relaxation weights. The colored lines are the history of the node-wise weights for each training iteration.

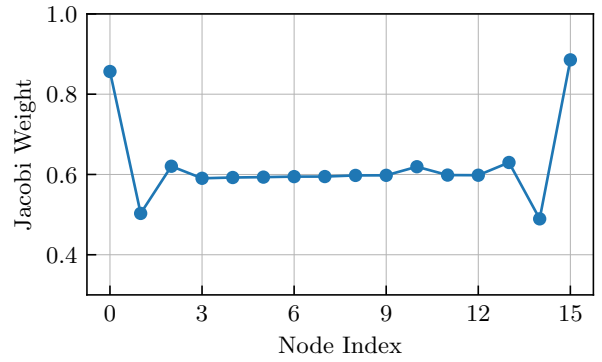


Figure 3. Final node-wise weight values for the Jacobi relaxation.

nodal weights at the two ends of the domain are maximized; for our problem setup this mimics the behavior of values being propagated from the boundaries inwards.

3.2. Heavyball Iteration

Polyak’s heavyball iteration (Polyak, 1964) is a two-step iterative method that uses the information from the last two iterates to generate the next approximation. It can be viewed as a gradient descent with a momentum term.

To minimize a differentiable function f , we consider the update step

$$\mathbf{x}^{(k+1)} = \mathbf{x}^{(k)} - \alpha \nabla_{\mathbf{x}} f(\mathbf{x}^{(k)}) + \beta (\mathbf{x}^{(k)} - \mathbf{x}^{(k-1)}), \quad (14)$$

for scalars $\alpha, \beta \in \mathbb{R}$. We then apply Equation (14) to solve systems of the form in Equation (10) by defining

$$f(\mathbf{x}; \mathbf{A}, \mathbf{b}) = \frac{1}{2} \mathbf{x}^T \mathbf{A} \mathbf{x} - \mathbf{b}^T \mathbf{x}. \quad (15)$$

Next, taking the gradient of f with respect to \mathbf{x} yields

$$\nabla_{\mathbf{x}} f(\mathbf{x}; \mathbf{A}, \mathbf{b}) = \mathbf{A} \mathbf{x} - \mathbf{b}, \quad (16)$$

where we have that if $\nabla_x f = \mathbf{0}$ then \mathbf{x} is a solution to the matrix system $\mathbf{A}\mathbf{x} = \mathbf{b}$.

Similarly, we consider the example problem in Section 3.1 by generating a 16×16 matrix \mathbf{A} and minimizing

$$\ell = \sum_{k=1}^K (\mathbf{h}_{12}(\mathbf{x}_k, \mathbf{0}; \alpha, \beta))^T \mathbf{A} \mathbf{h}_{12}(\mathbf{x}_k, \mathbf{0}; \alpha, \beta), \quad (17)$$

where $\mathbf{h}_L(\mathbf{x}_k, \mathbf{b}; \alpha, \beta)$ is the application of L rounds of heavyball iteration to \mathbf{x}_k with right-hand-side \mathbf{b} and parameters α, β . Again, the $\{\mathbf{x}_k\}$ is a set of K vectors in \mathbb{R}^N with unit-normally distributed entries.

We optimize the error after $\frac{3}{4}N$ iterations of the heavyball method. The parameter history as a function of training epoch is shown in Figure 4.

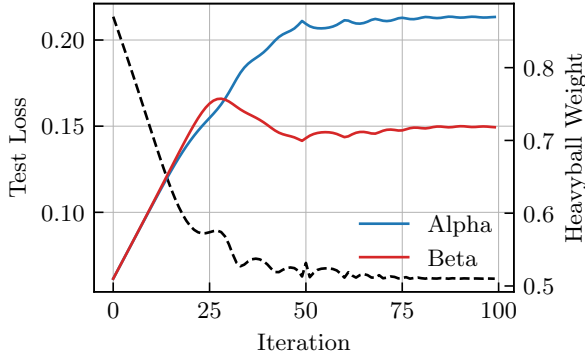


Figure 4. Parameter history for each heavyball training iteration, plotted along with the training loss.

3.3. Conjugate Gradient

The conjugate gradient (CG) method is another iterative solver for matrix equations of the form in Equation (10) when \mathbf{A} is SPD. While it typically exhibits faster convergence than both the Jacobi and heavyball methods, convergence can be accelerated further by passing an approximate inverse to \mathbf{A} , denoted by $\mathbf{M} \approx \mathbf{A}^{-1}$, with the assumption that \mathbf{M} is itself SPD, using the preconditioned conjugate gradient (PCG) method (Saad, 2003).

We extend the one-dimensional problem in Equation (7) to two dimensions via tensor product over the x and y dimensions, as in

$$\mathbf{A} = \mathbf{A}_{N_x \times N_y} = (\mathbf{A}_{N_x} \otimes \mathbf{I}_{N_y}) + (\mathbf{I}_{N_x} \otimes \mathbf{A}_{N_y}), \quad (18)$$

where \otimes denotes the standard matrix Kronecker product, and \mathbf{A}_N indicates a one-dimensional discretization with N interior grid points. For our test problem we use $N_x = N_y = 8$, resulting in a matrix shape $\mathbf{A} \in \mathbb{R}^{64 \times 64}$.

The goal is the construction of \mathbf{M} that suitably approximates the inverse to \mathbf{A} . We note that PCG requires a SPD

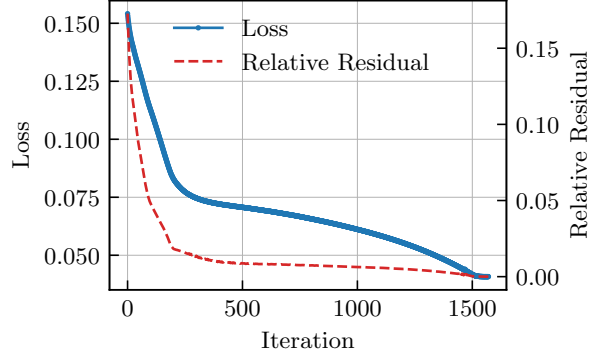


Figure 5. Loss history in constructing \mathbf{M} , the CG preconditioner. The blue line (left axis) is the loss and the red dashed line (right axis) is the relative residual.

preconditioner; to enforce this we instead directly learn a lower triangular \mathbf{L} and form \mathbf{M} like

$$\mathbf{M} = \mathbf{L}\mathbf{L}^T. \quad (19)$$

We do not directly constrain \mathbf{M} to be positive definite; indefinite or semidefinite preconditioners are unlikely to converge well and thus such a preconditioner will be avoided during optimization.

To find the entries in \mathbf{M} , we introduce the weighted loss

$$\ell = \sum_{i=1}^{N_{\text{it}}} \left(\frac{\gamma^{N_{\text{it}}-i}}{\sum_{j=1}^{N_{\text{it}}} \gamma^{N_{\text{it}}-j}} \right) \frac{\|\mathbf{r}^{(i)}\|_2}{\|\mathbf{b}\|_2}, \quad (20)$$

where N_{it} is the number of PCG iterations run (we use $N_{\text{it}} = 4$), $\mathbf{r}^{(i)}$ is the i th residual of the iteration, \mathbf{b} is the right-hand-side, and $\gamma \in (0, 1]$ is a scaling constant (we use $\gamma = 0.6$). With this form, we minimize the overall weighted sum of the residual history with later iterates being weighted more than earlier ones. Experimentally, we observe improved convergence of the optimization problem in comparison to minimizing only over the last iterate. This also avoids the problem of vanishing gradients as the number of iterations is increased, as gradient information is used from each intermediate iterate.

We run the optimization over a lower bidiagonal \mathbf{L} , which gives a tridiagonal $\mathbf{M} = \mathbf{L}\mathbf{L}^T$. The loss and final relative residual obtained during each training iteration are displayed in Figure 5, while the residual history with and without \mathbf{M} is shown in Figure 6.

3.4. Graph Neural Networks

The GCN layer (Kipf & Welling, 2017) is a graph convolutional layer that *convolves* node features on a graph, $G(\mathbf{A})$. Denoting the (weighted) adjacency matrix of the graph by $\mathbf{A} \in \mathbb{R}^{n \times n}$, and denoting $\mathbf{X}^{(i)} \in \mathbb{R}^{n \times C}$ as the

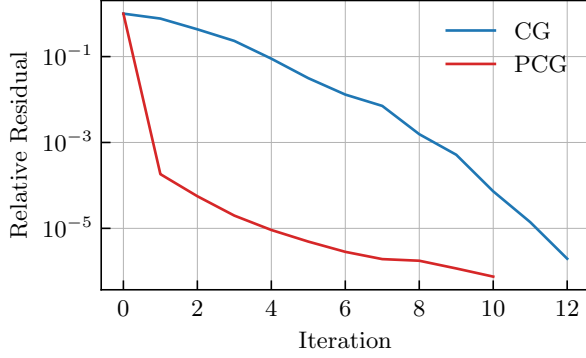


Figure 6. Relative residual history of a regular (non-preconditioned) CG and the preconditioner found by optimization.

C -dimensional node features at layer i , we represent the convolution of the node features as

$$\mathbf{X}^{(i+1)} = \tilde{\mathbf{D}}^{-\frac{1}{2}} \tilde{\mathbf{A}} \tilde{\mathbf{D}}^{-\frac{1}{2}} \mathbf{X}^{(i)} \Theta^{(i+1)}, \quad (21)$$

where $\Theta \in \mathbb{R}^{C \times F}$ is the weight matrix for the layer, $\tilde{\mathbf{A}} = \mathbf{A} + \mathbf{I}$, and $\tilde{\mathbf{D}}$ is the diagonal matrix extracted from $\tilde{\mathbf{A}}$.

We reimplement the GCN layer using our optimized underlying sparse matrix operations. Depending on the order of operations, computing the output in Equation (21) can be seen as a series of sparse-dense matrix multiplies (multiplying from right-to-left), or as two sparse-sparse multiplies followed by dense multiplies. In the following, we employ the former method.

Using this GCN layer, we reimplement the semi-supervised CiteSeer example from Kipf & Welling (2017). This dataset has 3327 nodes, 4732 edges, and 6 classes. We train a two-layer GCN with ReLU and sigmoid activations after the first and second layers and use a cross-entropy loss to optimize the predicted labels on each node, which follows the same setup as in Kipf & Welling (2017). Likewise, between each GCN layer is a dropout layer with $p = 0.5$, and we train with an Adam optimizer using a learning rate of 0.01, L2 regularization of 5×10^{-4} , and 16-dimensional representations for the hidden node features. This is trained for 200 epochs over 100 random initializations and training history can be seen in Figure 7.

As seen in Figure 8, we are able to match the roughly 70% classification accuracy on the CiteSeer dataset.

3.5. Optimized Domain Decomposition

In this section, we consider the learned domain decomposition solver from (Taghibakhshi et al., 2022). The method begins with an a priori partitioning of the matrix rows/columns, Ω , into S disjoint subdomains $\mathcal{D}_1, \mathcal{D}_2, \dots, \mathcal{D}_S$ such that $\mathcal{D}_i \cap \mathcal{D}_j = \emptyset \forall i, j$ s.t. $i \neq j$, and $\bigcup_i \mathcal{D}_i = \Omega$. We denote piecewise constant restriction operators from Ω to subdo-

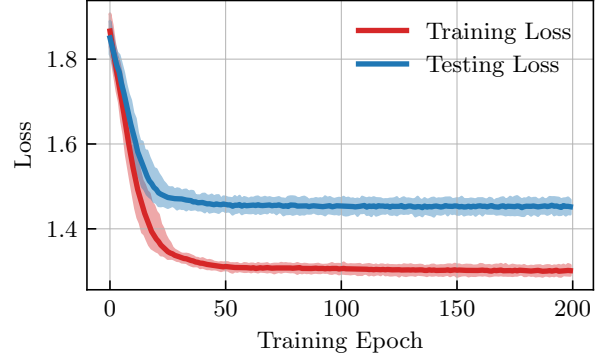


Figure 7. Loss history over training the GNN over the CiteSeer dataset. Averaged over 100 runs, lines denote mean while shaded regions are two standard deviations from mean.

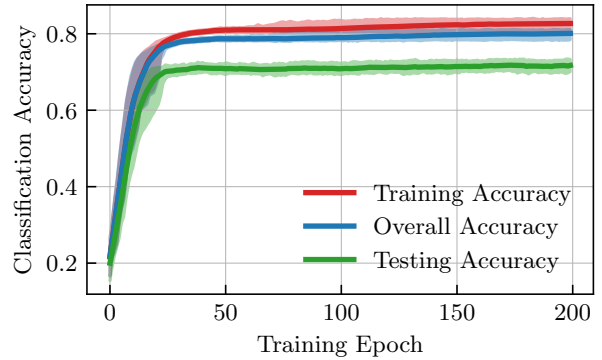


Figure 8. Classification accuracy of the networks per training epoch. Averaged over 100 runs, lines denote mean while shaded regions are two standard deviations from mean.

main \mathcal{D}_i by \mathbf{R}_i^0 . To allow for some overlap between domains, we additionally let \mathbf{R}_i^δ be the restriction to \mathcal{D}_i^δ , the union of \mathcal{D}_i and the set of nodes that have at most distance δ from its boundary. Note, however, that \mathbf{R}_i^0 and \mathbf{R}_i^δ may introduce different orderings to nodes on the local subdomain \mathcal{D}_i , thus we also define $\tilde{\mathbf{R}}_i^\delta$ to have the same shape and row ordering as in \mathbf{R}_i^δ but with nonzero rows only for nodes in \mathcal{D}_i itself: extended boundary node values are masked off.

Following standard RAS domain decomposition literature (Toselli & Widlund, 2005), we then form an approximate inverse or preconditioner to \mathbf{A} like

$$\mathbf{A}^{-1} \approx \mathbf{M}_{\text{DD}} = \sum_{i=1}^S \left(\tilde{\mathbf{R}}_i^\delta \right)^T \mathbf{A}_i^{-1} \mathbf{R}_i^\delta, \quad (22)$$

where \mathbf{A}_i is a projection (or re-discretization) of the full problem to subdomain \mathcal{D}_i^δ . We note, however, that one may obtain a better approximation if we instead use a modified $\tilde{\mathbf{A}}_i$,

$$\tilde{\mathbf{A}}_i = \mathbf{A}_i + \mathbf{L}_i, \quad (23)$$

where \mathbf{L}_i is some learned matrix containing entries only

on the subdomain *boundary*; we are, in essence, learning the interface or transmission conditions for each subdomain. To output L_i , we first obtain A and a set of node values d , defined as

$$d_i = \begin{cases} 1 & \text{node } i \text{ is along a subdomain boundary,} \\ 0 & \text{otherwise.} \end{cases} \quad (24)$$

These are then passed to a graph neural network consisting of multiple node and edge convolutions (see Appendix C from Taghibakhshi et al. (2022) for exact architecture) with learnable parameters θ to output a new matrix $\hat{L}^{(\theta)}$ such that $\text{mask}(\hat{L}^{(\theta)}) = \text{mask}(A)$. For each subdomain \mathcal{D}_i , we then mask $\hat{L}^{(\theta)}$ so that $L_i^{(\theta)}$ contains nonzero entries only between the boundary nodes in \mathcal{D}_i . This gives us the learned preconditioner

$$M^{(\theta)} = \sum_{i=1}^S \left(\tilde{R}_i^\delta \right)^T \left(R_i^\delta A \left(R_i^\delta \right)^T + L_i^{(\theta)} \right)^{-1} R_i^\delta. \quad (25)$$

To optimize the network parameters to output optimal interface conditions, we define the error propagation operator

$$T^{(\theta)} = I - M^{(\theta)} A, \quad (26)$$

as a theoretical bound on the decrease of error for each iteration of the domain decomposition solver. An obvious choice for a loss is to minimize over the spectral norm of $T^{(\theta)}$ as this would directly affect how fast the solver converges. Computing this can be difficult in practice, however. To avoid expensive eigendecompositions that may particularly cause trouble with gradient propagation, we instead use a stochastic approximation: let $\mathcal{X} = \{x_1, x_2, \dots, x_m\}$ be a set of m unit vectors in \mathbb{R}^n whose entries are uniformly distributed; we approximate the loss by a stochastic relaxation of the induced matrix norm,

$$\ell \approx \max_{x \in \mathcal{X}} \left\| \left(T^{(\theta)} \right)^k x \right\|_2, \quad (27)$$

where k is the number of solver iterations to train on. We thus have a loss that we can use to train the domain decomposition method in an end-to-end fashion. In their work, Taghibakhshi et al. (2022) are constrained to training on small problem sizes as their automatic differentiation package does not support the sparse-sparse product $M^{(\theta)} A$; both $M^{(\theta)}$ and A are stored in their dense representation for training the GNN. With the differentiable sparse kernels that we have introduced in Section 2, we reimplement their training routine using sparse operations where applicable; timing results showing a comparison of dense vs sparse operations are shown in Section 4.

4. Timings

To underscore the scalability that we obtain versus using dense operations only, we show timings for each of the examples from Section 3 for a variety of problem sizes as well as a comparison to using dense operations only, in Table 2. We note that the sparse implementations show excellent scalability when compared to the dense-only implementations: the Jacobi, Heavyball, and PCG examples can run in reasonable time until $N = 16,384$, while the dense counterparts begin to take large amounts of time, especially on CPU. In particular, the dense PCG implementation tends to scale like $\mathcal{O}(N^3)$ because of the $M = LL^T$ product that is used to form the preconditioner. Furthermore, the dense implementations are unable to run at all for $N = 65,536$, as too much memory is consumed storing the matrix representation and intermediate data for backpropagation. For the GCN example, we train the same network as described in Section 3.4 on four different datasets: Cora ($N = 2,708$), CiteSeer ($N = 3,327$), and PubMed ($N = 19,717$) datasets from Kipf & Welling (2017); Yang et al. (2016); and the Flickr ($N = 89,250$) dataset from Zeng et al. (2019). Here, N refers to the number of nodes present in the graph. Again, we see strong scaling in the sparse implementation of the graph network; in fact we do not even begin to saturate available GPU cores until the largest dataset is run – the running time until then is dominated largely by kernel launch overhead. The results for the domain decomposition method are particularly striking, as the existing dense implementation is unable to scale larger than problems of size $N = 5,929$ without running out of memory, whereas the sparse implementation continues to run for larger problems with roughly linear time complexity with respect to the problem size. Additional timing results for the matrix kernels themselves with comparison to other libraries are given in Appendix C.

5. Conclusions

In this work, we have described the implementation of a framework for automatically computing the gradient through computations with sparse matrix operations. We have stated the backward propagation update rules and described at a high level how one may efficiently implement them on CPUs and GPUs. We demonstrated a range of applications that can be optimized using these sparse matrix primitives. Finally, we presented timing and scaling results to show that our implementations are both scalable with respect to dense linear algebra routines, and competitive in the forward pass with other sparse linear algebra packages. There are numerous directions of future work that we envision from this paper: perhaps the most straightforward is the implementation of more complex sparse linear algebra operations such as eigensolver routines, linear least squares, etc. The implementation of a sparse direct solve routine

Table 2. Timings for training the various example problems for one training epoch, averaged over 5 runs. Entries with (–) indicate runs that did not complete due to insufficient memory needed for both forward and back-propagation. Units are in seconds.

Example	Impl.	Device	$N = 1,024$	$N = 4,096$	$N = 16,384$	$N = 65,536$
Jacobi	Sparse (ours)	CPU	0.042	0.040	0.064	0.112
		GPU	0.818	0.704	0.737	0.887
	Dense	CPU	0.154	5.762	362.499	–
		GPU	0.796	0.877	1.889	–
			$N = 1,024$	$N = 4,096$	$N = 16,384$	$N = 65,536$
Heavyball	Sparse (ours)	CPU	0.119	0.492	3.607	21.527
		GPU	0.856	1.400	3.395	7.542
	Dense	CPU	0.138	6.370	571.974	–
		GPU	0.800	1.190	13.182	–
			$N = 1,024$	$N = 4,096$	$N = 16,384$	$N = 65,536$
PCG	Sparse (ours)	CPU	0.851	2.832	11.137	33.840
		GPU	1.204	1.390	2.079	4.375
	Dense	CPU	8.977	510.795	32,585.736	–
		GPU	1.013	3.801	177.179	–
			$N = 2,708$	$N = 3,327$	$N = 19,717$	$N = 89,250$
GCN	Sparse (ours)	CPU	0.035	0.052	0.193	1.321
		GPU	0.723	0.708	0.758	0.987
	Dense	CPU	0.131	0.157	3.893	–
		GPU	0.748	0.701	0.784	–
			$N = 1,521$	$N = 2,916$	$N = 5,929$	$N = 8,100$
Domain Decomp.	Sparse (ours)	CPU	3.060	5.088	12.906	18.321
		GPU	1.516	1.817	3.106	3.979
	Dense	CPU	2.274	15.126	–	–
		GPU	0.971	2.262	–	–

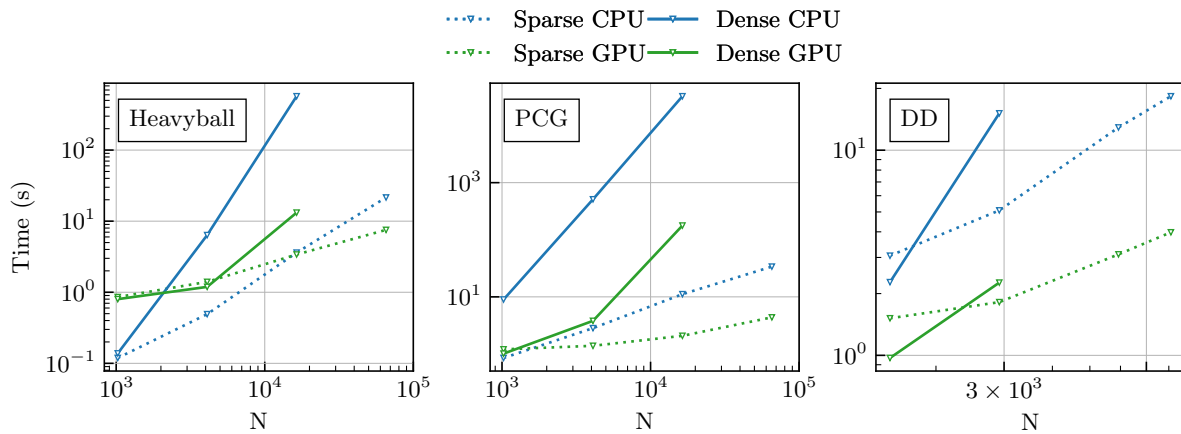


Figure 9. Timing results for the Heavyball, Preconditioned Conjugate Gradient, and Domain Decomposition applications. The sparse implementations exhibit lower algorithmic complexity as a function of N when compared to their respective dense implementations.

could be immensely useful and its implementation could follow scalable approaches such as in Gaihare et al. (2022).

Our reference PyTorch interface code can be found at <https://github.com/nicknytko/numml>.

Acknowledgments

This research was enabled in part by support provided by ACENET (www.ace-net.ca), and the Digital Research Alliance of Canada (alliancecan.ca). The work of SM was partially supported by an NSERC Discovery Grant.

References

- Abadi, M., Barham, P., Chen, J., Chen, Z., Davis, A., Dean, J., Devin, M., Ghemawat, S., Irving, G., Isard, M., Kudlur, M., Levenberg, J., Monga, R., Moore, S., Murray, D. G., Steiner, B., Tucker, P., Vasudevan, V., Warden, P., Wicke, M., Yu, Y., and Zheng, X. TensorFlow: A system for large-scale machine learning. In *12th USENIX Symposium on Operating Systems Design and Implementation (OSDI 16)*, pp. 265–283, 2016. URL <https://www.usenix.org/system/files/conference/osdi16/osdi16-abadi.pdf>.
- Baydin, A. G., Pearlmutter, B. A., and Radul, A. A. Automatic differentiation in machine learning: a survey. *CoRR*, abs/1502.05767, 2015. URL <http://arxiv.org/abs/1502.05767>.
- Bonfatti, F., Monaco, V., and Tiberio, P. Microwave circuit analysis by sparse matrix techniques. In *1973 IEEE G-MTT International Microwave Symposium*, pp. 41–43, 1973. doi: 10.1109/GMTT.1973.1123084.
- Bradbury, J., Frostig, R., Hawkins, P., Johnson, M. J., Leary, C., Maclaurin, D., Necula, G., Paszke, A., VanderPlas, J., Wanderman-Milne, S., and Zhang, Q. JAX: composable transformations of Python+NumPy programs, 2018. URL <http://github.com/google/jax>.
- Briggs, W. L., Henson, V. E., and McCormick, S. F. *A Multigrid Tutorial, Second Edition*. Society for Industrial and Applied Mathematics, second edition, 2000. doi: 10.1137/1.9780898719505. URL <https://epubs.siam.org/doi/abs/10.1137/1.9780898719505>.
- Dalton, S., Olson, L., and Bell, N. Optimizing sparse matrix—matrix multiplication for the GPU. *ACM Trans. Math. Softw.*, 41(4), oct 2015. ISSN 0098-3500. doi: 10.1145/2699470. URL <https://doi.org/10.1145/2699470>.
- Gaihare, A., Li, X. S., and Liu, H. GSoFa: Scalable sparse symbolic LU factorization on GPUs. *IEEE Transactions on Parallel and Distributed Systems*, 33:1015–1026, 4 2022. ISSN 15582183. doi: 10.1109/TPDS.2021.3090316.
- George, A., Gilbert, J. R., and Liu, J. W. H. (eds.). *Graph Theory and Sparse Matrix Computation*. Springer New York, 1993. doi: 10.1007/978-1-4613-8369-7. URL <https://doi.org/10.1007/978-1-4613-8369-7>.
- Giles, M. B. Collected matrix derivative results for forward and reverse mode algorithmic differentiation. *Lecture Notes in Computational Science and Engineering*, 64 LNCSE:35–44, 2008. ISSN 14397358. doi: 10.1007/978-3-540-68942-3_4/COVER. URL https://link.springer.com/chapter/10.1007/978-3-540-68942-3_4.
- Greenfeld, D., Galun, M., Kimmel, R., Yavneh, I., and Basri, R. Learning to optimize multigrid PDE solvers, 2019. URL <https://arxiv.org/abs/1902.10248>.
- Johnson, J. Derivatives, backpropagation, and vectorization. <http://cs231n.stanford.edu/handouts/derivatives.pdf>, September 2017.
- Kingma, D. P. and Ba, J. Adam: A method for stochastic optimization, 2014. URL <https://arxiv.org/abs/1412.6980>.
- Kipf, T. N. and Welling, M. Semi-supervised classification with graph convolutional networks. In *International Conference on Learning Representations*, 2017. URL <https://openreview.net/forum?id=SJU4ayYgl>.
- Kolda, T. G. and Bader, B. W. Tensor decompositions and applications. *SIAM Review*, 51(3):455–500, 2009. doi: 10.1137/07070111X. URL <https://doi.org/10.1137/07070111X>.
- Luz, I., Galun, M., Maron, H., Basri, R., and Yavneh, I. Learning algebraic multigrid using graph neural networks, 2020. URL <https://arxiv.org/abs/2003.05744>.
- Paszke, A., Gross, S., Massa, F., Lerer, A., Bradbury, J., Chanan, G., Killeen, T., Lin, Z., Gimelshein, N., Antiga, L., Desmaison, A., Köpf, A., Yang, E. Z., DeVito, Z., Raison, M., Tejani, A., Chilamkurthy, S., Steiner, B., Fang, L., Bai, J., and Chintala, S. PyTorch: An imperative style, high-performance deep learning library. *CoRR*, abs/1912.01703, 2019. URL <http://arxiv.org/abs/1912.01703>.
- Polyak, B. Some methods of speeding up the convergence of iteration methods. *USSR Computational Mathematics and Mathematical Physics*,

4(5):1–17, 1964. ISSN 0041-5553. doi:
[https://doi.org/10.1016/0041-5553\(64\)90137-5](https://doi.org/10.1016/0041-5553(64)90137-5).
URL <https://www.sciencedirect.com/science/article/pii/0041555364901375>.

Quarteroni, A., Sacco, R., and Saleri, F. *Numerical Mathematics*. Texts in Applied Mathematics. Springer, Berlin, Germany, 2 edition, October 2006.

Saad, Y. *Iterative Methods for Sparse Linear Systems*. Other Titles in Applied Mathematics. SIAM, second edition, 2003. ISBN 978-0-89871-534-7. doi: 10.1137/1.9780898718003. URL http://www-users.cs.umn.edu/~{ }saad/IterMethBook_2ndEd.pdf.

Su, J., Zhang, F., Liu, W., He, B., Wu, R., Du, X., and Wang, R. CapelliniSpTRSV: A thread-level synchronization-free sparse triangular solve on GPUs. pp. 1–11. ACM, 8 2020. ISBN 9781450388160. doi: 10.1145/3404397.3404400. URL <https://dl.acm.org/doi/10.1145/3404397.3404400>.

Taghibakhshi, A., Nytko, N., Zaman, T., MacLachlan, S., Olson, L., and West, M. Learning interface conditions in domain decomposition solvers. 5 2022. URL <http://arxiv.org/abs/2205.09833>.

Tao, Y., Deng, Y., Mu, S., Zhu, M., Xiao, L., Ruan, L., and Huang, Z. Atomic reduction based sparse matrix-transpose vector multiplication on GPUs. *Proceedings of the International Conference on Parallel and Distributed Systems - ICPADS, 2015-April*:987–992, 2014. ISSN 15219097. doi: 10.1109/PADSW.2014.7097920.

Toselli, A. and Widlund, O. B. *Domain Decomposition Methods — Algorithms and Theory*. Springer Berlin Heidelberg, 2005. doi: 10.1007/b137868. URL <https://doi.org/10.1007/b137868>.

Wu, Z., Pan, S., Chen, F., Long, G., Zhang, C., and Yu, P. S. A comprehensive survey on graph neural networks. *IEEE Transactions on Neural Networks and Learning Systems*, 32:4–24, 1 2021. ISSN 2162-237X. doi: 10.1109/TNNLS.2020.2978386. URL <https://ieeexplore.ieee.org/document/9046288/>.

Yang, Z., Cohen, W. W., and Salakhutdinov, R. Revisiting semi-supervised learning with graph embeddings, 2016. URL <https://arxiv.org/abs/1603.08861>.

Zeng, H., Zhou, H., Srivastava, A., Kannan, R., and Prasanna, V. GraphSAINT: Graph sampling based inductive learning method, 2019. URL <https://arxiv.org/abs/1907.04931>.

A. Software Versions

Our sparse kernels are compiled as a PyTorch extension written in C++17 using GCC, with the `-O2` flag enabled as the only non-default option. The list of library versions we use and compare against are detailed in Table 3.

Table 3. Software versions used for testing.

Library	Backend	Version
FlexiBLAS	BLIS	0.8.1
Python	CPython	3.10.2
SciPy		1.8.0
NumPy		1.22.2
CUDA		11.7
CuPy		11.2.0
PyTorch		1.13.0

B. Background

Unless noted, $\mathbf{A} \in \mathbb{R}^{n \times n}$ and $\mathbf{b}, \mathbf{x} \in \mathbb{R}^n$ represent the variables in the (sparse) system of linear equations

$$\mathbf{A}\mathbf{x} = \mathbf{b}. \quad (28)$$

For iterative solvers, \mathbf{x}_k denotes the approximate solution to Equation (28) at iteration k , along with residual $\mathbf{r}_k = \mathbf{b} - \mathbf{A}\mathbf{x}_k$, and error $e_k = \mathbf{x} - \mathbf{x}_k$.

Given a sparse matrix \mathbf{M} , let $\text{mask}(\mathbf{M})$ denote the *sparsity mask* of \mathbf{M} as in

$$[\text{mask}(\mathbf{M})]_{ij} = \begin{cases} 1 & m_{ij} \neq 0 \\ 0 & \text{otherwise} \end{cases}. \quad (29)$$

Letting \odot denote the standard Hadamard product, $\mathbf{A} \odot \text{mask}(\mathbf{M})$ then represents (sparse) matrix \mathbf{A} masked to the sparsity of \mathbf{M} . The sparsity mask also leads to the identity $\mathbf{M} \odot \text{mask}(\mathbf{M}) = \mathbf{M}$, and, by convention, if \mathbf{M} is dense then $\text{mask}(\mathbf{M})$ is also dense.

B.1. Chain Rule

For background, we recall the multivariate chain rule (Johnson, 2017) in Theorem B.1.

Theorem B.1. *Given function $f : \mathbb{R}^{n_x} \rightarrow \mathbb{R}$ and vectors $\mathbf{t} \in \mathbb{R}^{n_t}$ and $\mathbf{x}(\mathbf{t}) \in \mathbb{R}^{n_x}$, the partial derivative $\frac{\partial z}{\partial t_i}$ for $z = f(\mathbf{x}(\mathbf{t}))$ is given by*

$$\frac{\partial z}{\partial t_i} = \sum_{j=1}^{n_x} \frac{\partial f}{\partial x_j} \frac{\partial x_j}{\partial t_i}. \quad (30)$$

For the general case, we can extend Theorem B.1 for arbitrary tensor-valued functions, with tensors representing n -dimensional arrays (Kolda & Bader, 2009), as in Corollary B.2.

Corollary B.2. *Let I_1, I_2, \dots, I_N denote the indices of an N -mode tensor. Given function $f : \mathbb{R}^{I_1 \times I_2 \times \dots \times I_{N_X}} \rightarrow \mathbb{R}$, and tensors $\mathcal{T} \in \mathbb{R}^{J_1 \times J_2 \times \dots \times J_{N_T}}$ and $\mathcal{X}(\mathcal{T}) \in \mathbb{R}^{I_1 \times I_2 \times \dots \times I_{N_X}}$, the partial derivative $\frac{\partial z}{\partial t_{j_1, j_2, \dots, j_{N_T}}}$ for $z = f(\mathcal{X}(\mathcal{T}))$ is given by*

$$\frac{\partial z}{\partial t_{j_1, \dots, j_{N_T}}} = \sum_{i_1=1}^{I_1} \dots \sum_{i_{N_X}=1}^{I_{N_X}} \frac{\partial z}{\partial x_{i_1, \dots, i_{N_X}}} \frac{\partial x_{i_1, \dots, i_{N_X}}}{\partial t_{j_1, \dots, j_{N_T}}}. \quad (31)$$

From Corollary B.2, we denote the term on the left side in the summation as the *generalized gradient*:

$$[\nabla_{\mathcal{X}}(z)]_{i_1, i_2, \dots, i_{N_X}} = \frac{\partial z}{\partial x_{i_1, i_2, \dots, i_{N_X}}}. \quad (32)$$

This represents “the gradient of z with respect to \mathcal{X} .” Moreover, the value attains the same shape (dimensionality and size in each dimension) as \mathcal{X} itself.

Likewise, from Corollary B.2, we refer to the term on the right in the summation as the *generalized Jacobian*:

$$[\mathcal{J}_{\mathcal{T}}(\mathcal{X})]_{(i_1, i_2, \dots, i_{N_X}), (j_1, j_2, \dots, j_{N_T})} = \frac{\partial x_{i_1, i_2, \dots, i_{N_X}}}{\partial t_{j_1, j_2, \dots, j_{N_T}}}, \quad (33)$$

where the parentheses in the indexing are used only to emphasize that the first N_X indices are used for the input, while the last N_T indices are used for the output. From this, we have that Equation (31) can be alternatively denoted as the tensor contraction $\nabla_{\mathcal{X}}(z)^T \mathcal{J}_{\mathcal{X}(\mathcal{T})}$ over the indices i_1, i_2, \dots, i_{N_X} .

B.2. Reverse Mode Automatic Differentiation

Contemporary machine learning frameworks use *reverse-mode automatic differentiation* to compute gradient information, which is an efficient means of computing gradients of scalar-valued functions with respect to tensor-valued inputs (Baydin et al., 2015). The computation, in essence, is first done normally in a *forward pass*, with compositions of elementary functions being recorded into a *computation graph*. A second *backward pass* is then executed, tracing the computation graph backwards from the scalar output back to each input node and computing intermediate gradients at each step.

To help illustrate, we consider the function

$$f(\mathbf{x}, \mathbf{y}) = 2 \sin(\langle \mathbf{x}, \mathbf{y} \rangle), \quad (34)$$

for which we seek to evaluate the derivative with respect to the vectors \mathbf{x} and \mathbf{y} . At each node of the computation graph (see Figure 10), the gradient of the output is calculated with respect to the input of that particular node; this is then passed further back in the graph. Formally, letting z be

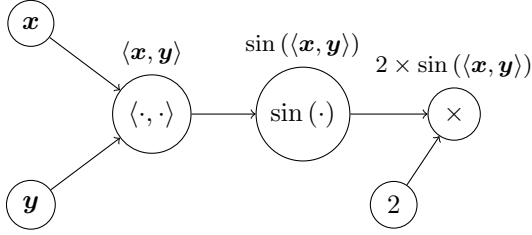


Figure 10. Example computation graph corresponding to evaluating Equation (34).

the scalar output of our computation and $\mathcal{Y} = f_i(\mathcal{X})$ be the computation done at node i , we find the intermediate gradient with the tensor contraction

$$\nabla_{\mathcal{X}}(z) = \nabla_{\mathcal{Y}}(z)^T J_{f_i(\mathcal{X})}(\mathcal{X}). \quad (35)$$

This operation is referred to as the *vector-Jacobian product* (VJP) in automatic differentiation. In the case that functions are vector valued ($\mathbb{R}^n \rightarrow \mathbb{R}^m$) this simplifies to vector-matrix products.

C. Sparse Kernel Timing Results

We present timing results for our implementation of the sparse kernels outlined in Section 2 along with a comparison of CPU and GPU (CUDA) timings in Table 4. For comparison, we have also included the respective *dense* operation in applicable cases, such as the dense matrix-vector (DMV) or dense-dense matrix-matrix product (DDMM). These dense implementations use the PyTorch built-in matrix routines. We also compare with NumPy/SciPy CPU and CuPy CUDA optimized versions for the forward passes.

Figure 11 highlights scaling results for the sparse matrix-vector product, sparse-sparse matrix product, and sparse-dense matrix product. These show the running time as a factor of the number of nonzeros in the matrix given in Equation (7), and indicate that forward and backward passes for the SpMV and SpSpMM are both linear in the nonzeros, while the forward and backward passes for the SpDMM are quadratic in the number of nonzeros. These timing results are run on a single compute node with one AMD Milan 7413 processor and one NVIDIA A100 GPU. Our CPU-based implementations are single threaded only, so for fair comparison we limit the amount of threads in the dense operations to one.

Optimized Sparse Matrix Operations for Reverse Mode Automatic Differentiation

Table 4. Timing results for CPU- and CUDA-based implementations. *Iterations* refers to the number of times the specific test was run (times listed are total wall-clock time elapsed); *N* refers to the problem size used, most usually the size of the matrix in one dimension. *GPU Speedup* is computed as CPU time / GPU time. Methods with *Sp* refer to *S*parse operations (ours), while *D* refers to *D*ense (PyTorch).

Test Name	ours CPU (s)	SciPy CPU (s)	ours GPU (s)	CuPy GPU (s)	GPU Speedup	Iter.	<i>N</i>
SpMV Forward	0.141	0.092	0.045	0.049	3.150	1000	32,768
SpMV Backward	0.595		0.198		3.003	1000	32,768
DMV Forward	143.441	143.614	2.985	2.983	48.058	1000	32,768
DMV Backward	1509.088		21.806		69.206	1000	32,768
SpSpMM Forward	0.184	0.065	0.048	0.032	3.798	100	16,384
SpSpMM Backward	2.150		0.293		7.336	100	16,384
SpDMM Forward	145.156	100.840	1.100	0.569	132.014	100	16,384
SpDMM Backward	303.903		4.923		61.736	100	16,384
DDMM Forward	190.113	202.030	0.985	0.921	193.097	2	16,384
DDMM Backward	597.621		2.846		210.020	2	16,384
Sp + Sp Forward	0.073	0.034	0.011	0.011	6.813	100	32,768
Sp + Sp Backward	0.133		0.025		5.227	100	32,768
D + D Forward	60.978	61.553	0.941	0.947	64.783	100	32,768
D + D Backward	123.519		2.596		47.580	100	32,768
SpTRSV Forward	0.030	32.746	4.710	0.767	0.006	100	32,768
SpTRSV Backward	13.462		10.997		1.224	100	32,768
DTRSV Forward	35.092	65.834	0.695	4.119	50.523	100	32,768
DTRSV Backward	863.779		3.499		246.855	100	32,768

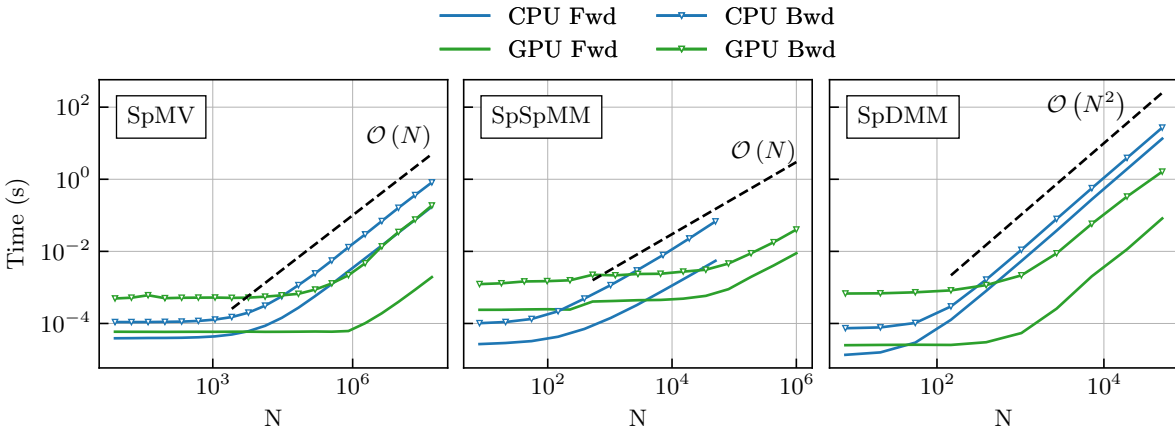


Figure 11. Scaling results for the forward and backward passes on several key sparse operations. The CPU running times are in blue, while the CUDA runtimes are in green. Triangle markers denote the backward pass routines.